Acta Cryst. (1996). B52, 471–478

Theoretical and Experimental (113 K) Electron-Density Study of Lithium Bis(tetramethylammonium) Hexanitrocobaltate(III)

RICCARDO BIANCHI,[a]* CARLO GATTI,[a] VICTOR ADOVASIO[b] AND MARIO NARDELLI[b]

[a]*Centro CNR per lo Studio delle Relazioni tra Struttura e Reattivita' Chimica, via Golgi 19, I-20133 Milano, Italy, and* [b]*Dipartimento di Chimica Generale ed Inorganica, Chimica Analitica e Chimica Fisica, Universita' degli Studi di Parma, Centro di Studio per la Strutturistica Diffrattometrica (CNR), viale delle Scienze 78, I-43100 Parma, Italy*

(*Received 24 July 1995; accepted 13 December 1995*)

Abstract

This paper presents an analysis of the crystal structure and the charge density, $\rho(\mathbf{r})$, for lithium bis(tetramethylammonium) hexanitrocobaltate(III) determined by the rigid pseudoatom model from accurate X-ray data measured at 113 K. This compound has also been investigated by an *ab initio* Hartree–Fock fully periodic approach. A comparison of the topological properties between the experimentally and theoretically derived density is also given. A notable agreement between experiment and theory is observed in the topological properties of the metal–ligand interaction and a close parallel between the orbital model description and the shape of the Laplacian distribution around the Co atom is outlined. The results confirm the typical 3*d*-electron distribution of octahedral Co^{III} complexes in a low-spin state and the presence of four C—H···O hydrogen bonds in the crystal structure. Important differences between experiment and theory remain for the Laplacian and the parallel curvature (λ_3) values at the C—N and N—O bond critical points. The atomic charges derived from the Quantum Theory of Atoms in Molecules are remarkably close to the formal values.

1. Introduction

Metal coordination compounds are of great chemical interest and much of what we know about the bonding in these compounds is derived from the analysis of their varied geometries or deduced from spectroscopic measurements. The electron-density determination is known to be a powerful tool to add chemical and physical information to that obtained by other techniques. For this reason, we have studied the electron-density distribution of $Li[N(CH_3)_4]_2[Co(NO_2)_6]$ determined both experimentally at 113 K by the multipole-expansion method (Stewart, 1976) and theoretically by the periodic Hartree–Fock method (Pisani, Dovesi & Roetti, 1988).

Two previous studies on Co^{III} complexes, reported by Ohba, Toriumi, Sato & Saito (1978) and Morooka, Ohba, Saito & Miyamae (1991), were based on the analysis of the deformation density (DD). These studies were mainly aimed at the determination of the asphericity of nonbonding 3*d*-electrons around the octahedrally coordinated transition-metal atom and of the electron-density distribution in the nitro group.

In this work we perform a topological analysis (Bader & Essen, 1984; Bader, 1990) and a comparison of the total experimental density with suitable theoretical densities in order to characterize the interaction between atoms in the title crystal. By proceeding in this way experiment and theory are *directly* compared in terms of the properties of an observable, using an approach (Bader, 1990) rooted in quantum mechanics. Some of the problems (Ruedenberg & Schwarz, 1990) inherent to DD studies are *a priori* avoided; neither the choice of the most appropriate promolecule density nor the resort to a given orbital model as an interpretative tool is needed in this framework.

Our study mainly focuses on the analysis of the aspherical 3*d*-electron distribution around the Co atom, the metal–ligand interaction, the bond nature in the coordinated NO_2^- group and the characteristics of the C—H···O interactions.

2. Calculations

The present work employs a set of X-ray data collected at 113 K from a small pseudooctahedral crystal of $Li[N(CH_3)_4]_2[Co(NO_2)_6]$. This compound crystallizes in the trigonal lattice with space group $P\bar{3}m1$ and $Z = 1$. Full details of the conventional crystal structure analysis were reported in a previous paper (Adovasio, Lina, Nardelli & Pelizzi, 1994).

2.1. *Refinement*

The quantity minimized in the multipole refinement was $\Sigma w(|F_o|^2 - k^2|F_c|^2)^2$ based on 3662 independent reflections up to $\sin\theta/\lambda$ of 1.361 Å^{-1} and weights $w = 1/\sigma^2(F_o^2)$. Extinction corrections were not introduced and the effects of anomalous dispersion were

considered only for the Co atom. *VALRAY* (Stewart & Spackman, 1983) estimates the scale factor k by the sum of the monopole populations divided by $F(000)$. The final aspherical fit to X-ray data was obtained with the following multipole model. Each pseudoatom is assigned a small finite multipole expansion of the atomic form factor (generalized scattering factor model or g.s.f. model) with a variable population parameter for each surface harmonic. The multipole expansion included two monopoles (one termed 'inner' and the other 'outer') and the higher terms were up to the hexadecapole level, except for Li (only two monopoles) and H atoms (a monopole and a dipole). The monopoles on heavy atoms consist of shells constructed from the canonical SCF s-, p- and d-orbitals (Clementi & Roetti, 1974). Each H monopole was a single shell, given by $\exp(-2.48r)$. For the higher multipoles, exponential radial functions with fixed standard molecular exponents (Hehre, Ditchfield, Stewart & Pople, 1970) were used for all atoms. The radial exponents of Co were allowed to vary in the refinement procedure and their final values were 3.8(5) and 7.6(2) $Å^{-1}$ for the quadrupole and hexadecapole functions, respectively. A single 'inner' monopole parameter was refined for the O, N and C atoms. The 'outer' monopole parameter of Li was fixed to zero as it was not possible to estimate it from the multipole refinement, while other electronic parameters were taken to be equal to zero because of the site symmetries ($\bar{3}m$ for Co and Li, $3m$ for C2 and N2 and m for O1, O2, N1, C1, H12 and H21). The nuclear positions of the H atoms were obtained by a multipole refinement assuming the H atoms are polarized in the direction of the atom to which they are bonded. Each atomic nucleus was weighted by the thermal function which was considered isotropic for H atoms and anisotropic for the other atoms. We stress that in the model chosen the nonspherical electron density rigidly follows the motion of the nucleus to which it is assigned. For comparison purposes, the conventional independent-atom model (IAM) was also considered. The scattering factors for the neutral spherical atoms were calculated from the wave functions of Clementi & Roetti (1974). The weights, $w = 1/\sigma^2(F_o^2)$, used in all refinements, are different from those used in the previous conventional structure analysis on F^2 (Adovasio *et al.*, 1994). All calculations based on X-ray data were performed using a modified version of the *VALRAY* program (Stewart & Spackman, 1983).

2.2. *X-ray properties*

The total electron density, $\rho(\mathbf{r})$, based on the g.s.f. model, was calculated with a direct space lattice sum. The gradient and Hessian of $\rho(\mathbf{r})$ were also computed with a direct space lattice sum. The topology of $\rho(\mathbf{r})$ can be fully described by its critical points, where the gradient of $\rho(\mathbf{r})$ vanishes (Bader & Essen, 1984). Critical points were located by the Newton–Raphson procedure in direct space.

2.3. *Ab initio properties*

For comparison purposes, the theoretical electron density was also evaluated, using the experimental geometry and the *ab initio* Hartree–Fock periodic approach, as implemented in the *CRYSTAL92* program (Dovesi, Saunders & Roetti, 1992). The adopted basis set is a modified 3-21G basis (Hehre, Radom, Schleyer & Pople, 1986). In order to avoid problems of the linear dependence of basis set functions, the most diffuse *sp* valence shells of Co and Li (exponents 0.037 and 0.029, respectively) were dropped and their innermost valence shells were split. By this procedure the total number of basis set functions equals that of the standard 3-21G basis. C, N and O atoms were then supplemented with one set of *d* polarization functions and Gaussian exponents as in the standard 6-31G* basis. The resulting number of basis functions in the cell is 476 and the amount of disk space required to store all the monoelectronic and bielectronic integrals was ~1.15 Gbytes.

The topological analysis of the theoretical charge density was carried out in a fully automatic way, using the *TOPOND* program (Gatti, Saunders & Roetti, 1994), interfaced to *CRYSTAL92*.

3. Results and discussion

3.1. *Crystal structure*

The octahedral $[Co(NO_2)_6]^{3-}$ anions are linked by the Li^+ cations along the $\bar{3}$ axis with Co at the (0,0,0) and Li^+ at the $(0,0,\frac{1}{2})$ symmetry centres. The Li^+ cation is surrounded by an octahedron of O atoms. The octahedra have symmetry $\bar{3}m$. The $[N(CH_3)_4]^+$ cations are packed along the threefold axes, surrounded by the O atoms from the nitro groups and involved with them in C—H···O interactions. A packing diagram and the ion structures are shown in Figs. 1(*a*) and (*b*). The final agreement factors and some other refinement information are listed in Table 1.* No relevant residual features are found in the difference-Fourier synthesis after multipole refinement. Bond lengths and angles, along with C—H···O interactions, are given in Tables 2 and 3, respectively. The bond distances and angles for heavy atoms (Table 2), derived from the multipole model, are significantly different from those obtained from the IAM. Furthermore, the discrepancies are largest for the geometrical data involving H atoms. The C—H···O contacts calculated from the aspherical

* Lists of atomic coordinates and anisotropic displacement parameters for conventional and multipole refinements have been deposited with the IUCr (Reference: CR0508). Copies may be obtained through the Managing Editor, International Union of Crystallography, 5 Abbey Square, Chester H1 2HU, England.

Table 1. *Refinement information*

	IAM	Multipole
N_o (number of reflections)	3662	3662
N_p (number of parameters)	45	106
$S = [\Sigma w(\|F_o\|^2 - k^2\|F_c\|^2)^2/(N_o - N_p)]^{1/2}$	2.589	1.646
$wR(F^2) = [\Sigma w(\|F_o\|^2 - k^2\|F_c\|^2)^2/\Sigma w\|F_o\|^4]^{1/2}$	0.0674	0.0431
$R(F^2) = \Sigma\|\|F_o\|^2 - k^2\|F_c\|^2\|/\Sigma\|F_o\|^2$	0.0444	0.0288
k (scale factor)	1.004 (1)	1.016 (3)
$[\Delta(p)/\sigma(p)]_{max}$	<0.001	<0.002

model are systematically shorter than the corresponding ones of the IAM model, thereby strengthening the rôle of hydrogen bonds in the crystal packing (see Table 3 and Fig. 1*b*).

3.2. *Electron density*

The most interesting topographical features of the electron-density function, $\rho(\mathbf{r})$, are determined by its critical points (CP's), where the gradient vanishes. CP's

Table 2. *Relevant bond distances (Å) and angles (°) from conventional (IAM) and multipole refinements*

	IAM	Multipole
Co—N1	1.9610 (2)	1.9655 (2)
O1—N1	1.2453 (4)	1.2399 (4)
O2—N1	1.2284 (4)	1.2263 (4)
N2—C1	1.4951 (4)	1.4946 (4)
N2—C2	1.4978 (10)	1.4958 (8)
Li—O1	2.0288 (2)	2.0299 (2)
C1—H11	0.973 (6)	1.087 (11)
C1—H12	1.042 (8)	1.077 (14)
C2—H21	0.902 (8)	1.057 (13)
Li—O1—N1	126.33 (2)	126.59 (2)
O1—N1—O2	118.80 (3)	119.19 (3)
Co—N1—O2	118.44 (2)	118.23 (2)
Co—N1—O1	122.76 (2)	122.58 (2)
C1—N2—C2	109.36 (3)	109.48 (3)
N2—C1—H11	104.7 (5)	108.0 (7)
N2—C1—H12	112.9 (4)	109.3 (5)
H11—C1—H11^{i}	113.6 (6)	110.1 (8)
H11—C1—H12	110.4 (4)	110.7 (5)
N2—C2—H21	106.3 (5)	108.6 (7)
H21—C2—H21^{ii}	112.4 (5)	110.4 (8)

Symmetry codes: (i) $1-y, 1-x, z$; (ii) $y-x, 1-x, z$.

Table 3. *Hydrogen-bond interactions (Å, °)*

First row, IAM refinement; second row, multipole refinement.

D—H···A	H···A	D···A	D—H···A
C1—H11···O1^{i}	2.703 (6)	3.6055 (3)	154.6 (6)
	2.583 (12)	3.6066 (3)	156.7 (7)
C1—H12···O2^{ii}	2.549 (6)	3.2531 (5)	124.4 (3)
	2.519 (9)	3.2512 (5)	124.4 (4)
C2—H21···O1^{iii}	2.644 (8)	3.5414 (3)	173.2 (7)
	2.498 (13)	3.5430 (1)	169.7 (10)
C2—H21···O2^{iii}	2.733 (8)	3.4747 (7)	140.2 (7)
	2.591 (13)	3.4762 (5)	140.9 (9)

Symmetry codes: (i) $x-y, x, 1-z$; (ii) $-y, x-y, 1+z$; (iii) $x, 1+y, z$.

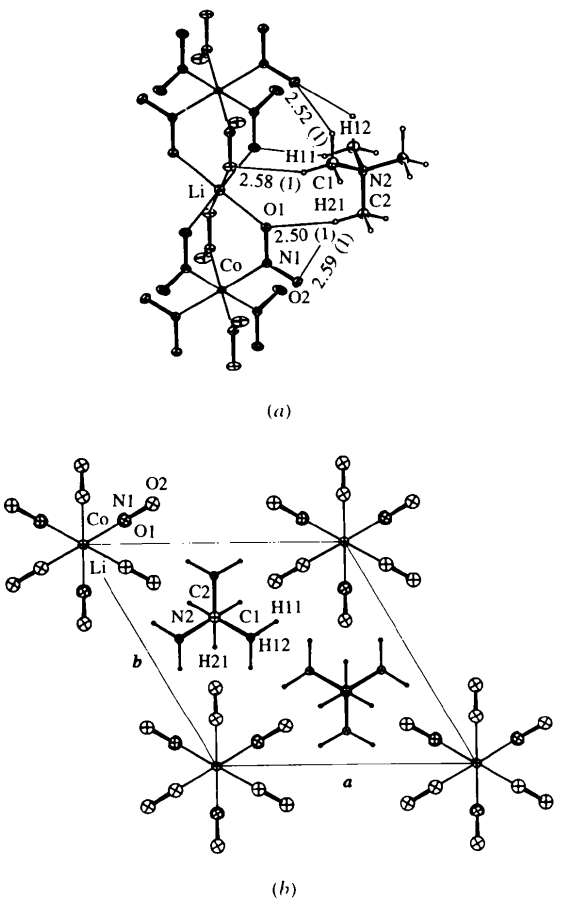

Fig. 1. (*a*) *ORTEP*II (Johnson, 1976) drawing of the molecular structure at 113 K. Ellipsoids are drawn at the 50% probability level. (*b*) Projection of the unit-cell contents (Å) along **c**.

can generally be classified in terms of invariants of the Hessian or curvature matrix $\mathbf{H}_p$ at the critical point. These invariants are the rank m (the number of nonzero eigenvalues), the signature n (the difference between the number of positive and negative eigenvalues) and the eigenvalues λ_1, λ_2 and λ_3 of the matrix $\mathbf{H}_p$. The nature of a generic critical point is therefore indicated by the pair (m, n); for a nondegenerate critical point ($m = 3$), only four different CP's are allowed. They are referred to as (3,−3), (3,−1), (3,+1) and (3,+3) and are associated with nuclei, bonds, rings and cages of the molecular structure, respectively (Bader, 1990). A given atomic interaction present in a molecule or in a crystal is then defined and characterized by the properties of the associated (3,−1) critical point, *i.e.* a bond critical point (BCP). A BCP is such that the density attains its minimum value along the bond path, a line connecting two nuclei, where $\rho(\mathbf{r})$ is a maximum with respect to any lateral displacement from the line.

Negative (positive) values of the electron density Laplacian, $\nabla^2\rho_b = \lambda_1 + \lambda_2 + \lambda_3$, are associated with molecular regions where the charge is locally concentrated (depleted). It has been demonstrated (Bader & Essen, 1984) that atomic interactions fall into two broad general classes, closed-shell and shared interactions. Covalent and polar bonds (shared interactions) are caused by a contraction of $\rho(\mathbf{r})$ towards the bond path and are characterized by large negative density curvatures in the direction perpendicular to this path and a consequent negative Laplacian at the BCP. Ionic bonds, hydrogen bonds and van der Waals interactions (closed-shell interactions) are dominated by the contraction of the electron density towards each of the nuclei. The positive Laplacian at the BCP is determined by dominance of the positive curvature λ_3 of $\rho(\mathbf{r})$, parallel to the bond path. The density value at the BCP, ρ_b, can be related to the bond order (Bader, Slee, Cremer & Kraka, 1983) and the ratio of the two negative curvatures at the BCP gives a measure of the deviation of the electron density from axial symmetry. This is termed ellipticity and is defined as $\varepsilon = \lambda_1/\lambda_2 - 1$. A detailed survey on the use of the topology of the electron density to assign and characterize both primary and secondary atomic interactions in crystals is presented by Tsirelson, Zou, Tang & Bader (1995).

Fig. 2. shows the total electron density derived from (*a*) pseudoatoms at rest and (*b*) from *ab initio* calculation in the mirror plane parallel to **c** and containing the Li, Co and NO_2^- ions. Inspection of the multipole $\sigma(\rho)$ map in the same plane indicates that the e.s.d. is below 0.06 e Å^{-3} in the bonding regions. Fig. 2 indicates a qualitative agreement between the experimental and the theoretical map; the presence of saddle points related to the expected chemical interactions is clearly evidenced in both the maps. Fig. 3 reports the experimental and theoretical Laplacian of $\rho(\mathbf{r})$ in the same plane as Fig. 2. A very good general agreement in the intermolecular regions as well as in the description of the Co and Li atom interactions with the NO_2^- group is observed. On the other hand, the N—O bonds appear to be described somewhat differently in the two maps. The metal–ligand interactions are also illustrated (Fig. 4) in a plane containing four of the six nitrogen atoms coordinated around the Co atom.

Table 4 summarizes the (3,−1) BCP properties of the title compound derived from the multipole model and from the theoretical density at the experimental geometry. The first important result is that the multipole density exhibits the same number and same type of CP's of the theoretical density, for both intra- and intermolecular interactions. Furthermore, a similar description of chemical interactions is also recovered by the two models. Shared interactions (CN, NO and CH bonds) are correctly described by the negative value of the Laplacian at the BCP. For both models, the N1—O2 bond has larger ρ_b and $|\nabla^2\rho_b|$ values than N1—O1, in agreement with the shorter bond length of N1—O2 (Table 2). In addition, the higher double-bond character of N1—O2 is indicated by its greater ellipticity value, confirming that the first of the two following resonance structures is more relevant.

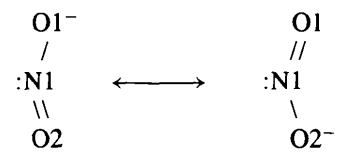

The major discrepancies between the two models concern the value of the λ_3 curvature for the C—N and N—O interactions. The experimental estimates of λ_3 are approximately twice as large as the theoretical

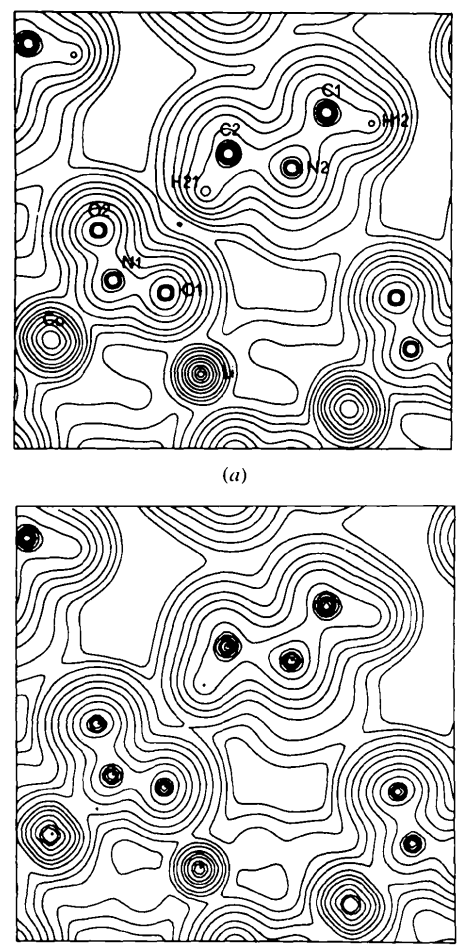

(*a*)

(*b*)

Fig. 2. Total electron density in the mirror plane parallel to **c** and containing the NO_2^- ion calculated (*a*) from the multipole model and (*b*) from the RHF/3-21G* wavefunction. The contour values (in a.u.) increase from the outermost one inwards in steps of 2×10^n, 4×10^n and 8×10^n, with n beginning at −3 and increasing in steps of 1.

ones. The observed differences in the λ_3 curvatures are likely to arise from the combined effect of the following factors: the different locations of BCP's (the theoretical BCP's are significantly shifted towards the less electronegative atom); the harmonic approximation for atomic thermal motion and the limited flexibility of the radial functions adopted in the multipole model; the smallness of the basis set employed and the neglect of the electron correlation in the theoretical calculations. We would briefly comment on these points. In a previous study on L-alanine (Gatti, Bianchi, Destro & Merati, 1992) a closer agreement between experiment and theory, in the description of the polar interactions, was found when the *ab initio* properties were evaluated at the experimental BCP locations. A less satisfactory behavior was observed in the present case. Fig. 5 compares the experimental and theoretical profiles of ρ and λ_3 along the N1—O2 and C2—N2 bond paths. The largest discrepancy is found for the λ_3 curvature along N1—O2; in fact, the experimental curvature remains much larger than the theoretical over a broad interval around the BCP. The evaluation of the theoretical λ_3 at the experimental BCP improves (worsens) the agreement between the λ_3 curvatures in the case of the C2—N2 (N1—O2) bond, the opposite being true when the experimental λ_3 is evaluated at the theoretical BCP. In order to improve the outcome of the multipolar analysis, additional refinements were carried out by introducing, either separately or together, the following model changes: (*a*) dipole and quadrupole radial functions for C, N and O, and also octopole and hexadecapole functions for Co were constructed with many rather than with a single exponential (Clementi & Roetti, 1974); (*b*) third (for C, N and O) and fourth (for Co) anharmonic thermal parameters were added, as defined in the Gram–Charlier expansion. However, the revised multipole models do not significantly improve the agreement between theory and experiment for any of the topological descriptors investigated. It has also been claimed (Howard, Hursthouse, Lehman & Poyner, 1995) that (owing to the shortcomings inherent to multipole models) CP properties for experimental and *ab initio* charge distributions are brought to a better agreement, when the latter are projected into the same multipole model as the experiment. However, our results for the C—N interactions are comparable, or even of better quality, than those reported by Howard *et al.* (1995) for L-dopa, in spite of the fact that the multipolar refinement step was not performed on our

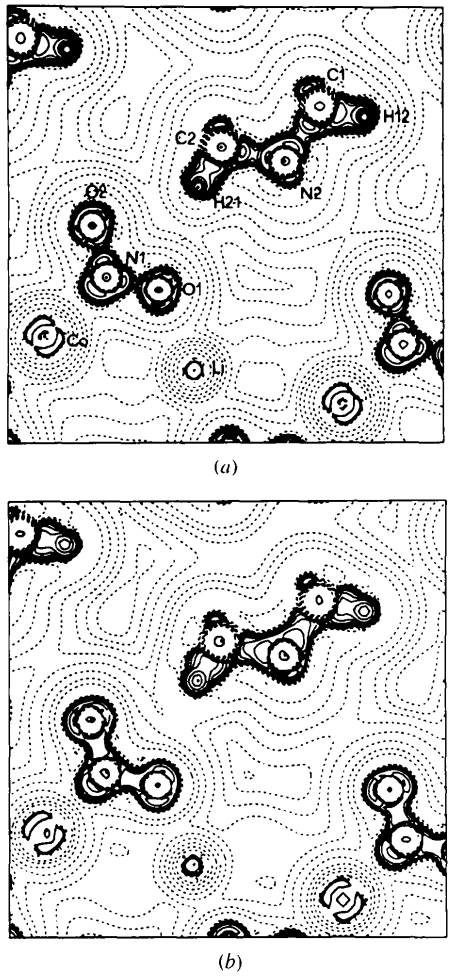

(*a*)

(*b*)

Fig. 3. (*a*) Experimental and (*b*) RHF/3-21G* Laplacian of the total electron density in the same plane as Fig. 2. Positive values of $\nabla^2\rho$ are denoted by dashed contours, negative values by solid contours. The negative and positive values of contours are drawn as in Fig. 2.

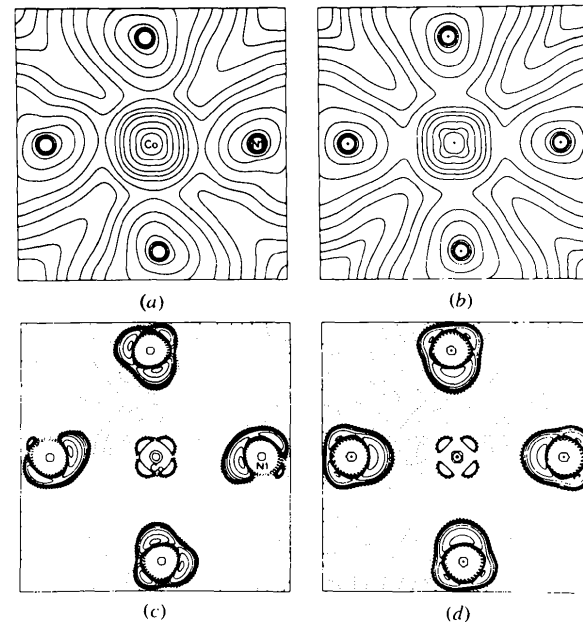

(*a*) (*b*) (*c*) (*d*)

Fig. 4. (*a*, *c*) Experimental, and (*b*, *d*) RHF/3-21G* maps of $\rho(\mathbf{r})$ and $\nabla^2\rho(\mathbf{r})$. The maps are drawn in a plane containing four of the six N atoms coordinated around cobalt. The contours are as in Fig. 2.

Table 4. *Bond critical point properties*

The first row gives values for $\rho(\mathbf{r})$ calculated from multipole refinement. The second row gives values derived from RHF/3-21G* *ab initio* calculation. R_x (Å) is the distance between the x atom and the BCP. The electron density ρ_b is in e Å^{-3} and the Laplacian $\nabla^2\rho_b$ is in e Å^{-5}.

x—y	Bond distance	R_x	ρ_b	$\nabla^2\rho_b$	λ_1	λ_2	λ_3	ε
Intramolecular interactions								
Co—N1	1.966	0.929	0.50 (1)	12.1 (1)	−2.8	−2.6	17.5	0.11
		0.906	0.62	13.0	−1.7	−1.4	16.1	0.14
N1—O1	1.240	0.597	3.19 (4)	−7.5 (10)	−30.3	−28.1	50.9	0.08
		0.555	3.28	−35.7	−31.6	−28.2	24.1	0.12
N1—O2	1.226	0.602	3.44 (4)	−11.9 (10)	−37.9	−31.6	57.7	0.20
		0.544	3.39	−37.4	−32.8	−28.7	24.1	0.14
C1—N2	1.495	0.659	1.83 (3)	−12.2 (8)	−15.2	−13.0	16.0	0.17
		0.500	1.59	−10.6	−9.4	−9.4	8.0	0.00
C2—N2	1.496	0.647	1.70 (6)	−12.4 (8)	−12.8	−12.8	13.3	0.00
		0.494	1.57	−9.2	−8.7	−8.7	8.4	0.00
Li—O1	2.030	0.804	0.110 (2)	3.81 (2)	−0.70	−0.69	5.20	0.01
		0.763	0.148	4.83	−0.96	−0.96	6.75	0.02
C1—H11	1.087	0.713	1.94 (6)	−11.5 (12)	−17.5	−16.7	22.7	0.05
		0.712	1.91	−23.6	−18.3	−17.6	12.3	0.06
C1—H12	1.077	0.721	1.78 (4)	−17.0 (21)	−18.1	−17.7	18.8	0.03
		0.705	1.96	−25.1	−19.3	−18.6	12.8	0.04
C2—H21	1.057	0.641	2.04 (6)	−21.9 (12)	−19.5	−18.7	16.3	0.04
		0.687	2.03	−26.5	−20.0	−19.0	12.5	0.05
C—H···O interactions								
H11···O1	2.583	1.152	0.022 (1)	0.36 (1)	−0.04	−0.01	0.41	3.00
		1.046	0.040	0.72	−0.24	−0.24	1.20	0.12
H12···O2	2.519	1.111	0.050 (4)	0.77 (2)	−0.16	−0.15	1.08	0.07
		1.065	0.047	0.96	−0.24	−0.24	1.44	0.26
H21···O1	2.498	1.103	0.035 (2)	0.66 (2)	−0.21	−0.09	0.96	1.33
		0.989	0.054	1.20	−0.21	−0.21	1.69	0.01
H21···O2	2.591	1.163	0.034 (2)	0.59 (2)	−0.17	−0.08	0.84	1.13
		1.047	0.040	0.72	−0.24	−0.24	1.20	0.18

theoretical data. We stress that, at variance with the L-dopa case, our theoretical data are derived from a fully periodic approach and therefore include a proper description of the crystal field effects. Finally, we comment on the possible inadequacies of our theoretical calculations. A detailed study of basis set effects on the topology of the electron density in the urea crystal (Gatti, Saunders & Roetti, 1993) has shown that the observed changes in the λ_3 curvature may even exceed 40% in the series 6-N1G, 6-N1G*, 6-N1G** ($N = 2, 3$). However, these changes do not follow a well defined trend for the class of polar bonds. For example, on passing from the 6-21G* to the 6-31G* basis set, the C—O bond has its λ_3 curvature increased while the C—N bond has the same curvature substantially decreased. The basis set adopted in the present study (3-21G*) predicts values of the topological descriptors for the urea crystal which are intermediate between those obtained with 6-21G* and 6-31G* basis sets. On the other hand, Coulomb correlation plays a less important rôle. It has been shown (Gatti *et al.*, 1992; Gatti, MacDougall & Bader, 1988) that the effect of Coulomb correlation on the topology of the molecular charge distributions is to slightly change (by ~1%) the ρ_b values and to increase or decrease (by ~10–20%) the λ_3 values for covalent and polar interactions, respectively.

For the closed-shell interactions (Co—N1, Li—O1 and C—H···O) the properties of the $\rho(\mathbf{r})$ at the associated BCP reflect their peculiar topological characteristics: a low value of ρ_b and a positive $\nabla^2\rho_b$ value with small and equal perpendicular curvatures (λ_1 and λ_2) and a dominant parallel curvature λ_3. Experiment and theory are indeed in noticeable agreement in describing the metal–ligand, Co—N1 and the iondative Li—O1 interactions (see Table 4).

In the octahedral field of $[Co(NO_2)_6]^{3-}$, the five 3*d*-orbitals will be split into the three t_{2g}-orbitals of lower energy and two e_g-orbitals of higher energy. The total t_{2g}-orbital charge density has eight lobes on the diagonals of a cube, while that associated with e_g-orbitals has six lobes pointing towards the faces of a cube (for a representation of the total charge density associated with e_g- and t_{2g}-orbitals in an octahedral environment, see Saito, 1979). The Laplacian distribution around the Co atom (Figs. 3 and 4) enlightens the correspondence between an observable ($\nabla^2\rho$) and the orbital model. Fig. 3 corresponds to a section through a face diagonal of the cube around an octahedrally coordinated cobalt and shows the lone pair of the N1 atom oriented towards the electron-deficient Co

e_g-orbital to form a coordination bond. In the language of quantum theory of atoms in molecules [QTAM (Bader, 1990)], the ligand–metal interaction results from the interaction of the charge concentration (CC) associated with the N1-atom lone pair with one of the six charge depletions (CD's) on the Co atom, arising from the emptiness of the two e_g-orbitals. Two such CD's are shown in Fig. 3, as expected on the basis of the orbital model. The maps of Fig. 4 are sections of the cube around an octahedrally coordinated cobalt, bisecting four edges and containing the center of four faces. In Figs. 4(*c*) and (*d*) the remaining four CD's associated with the electron deficient e_g-orbitals are shown, each one pointing towards the corresponding CC of the N1-atom lone pairs. The CC's around the Co atom in Figs. 3 and 4 are associated with the filled t_{2g}-orbitals and, again, show the expected shape and multiplicity on the basis of the orbital model. The relatively larger inequality of the two N—O bonds, as obtained from experiment, reflects small distortion of the CC associated with the N1 lone pairs. Fig. 3(*a*) shows that the greater CC of the N1—O2 bond slightly displaces the N-atom lone-pair CC towards the smaller N1—O1 CC, in order to minimize electron pair repulsions. This effect is made more evident in Fig. 4(*c*) and is also forewarned by the shape of the corresponding electron density in Fig. 4(*a*). The features of the Laplacian distribution around the Co atom closely resemble those found in the deformation maps for $[Co(NH_3)_6][Co(CN)_6]$ (Iwata & Saito, 1973) and $K_2Na[Co(NO_2)_6]$ (Ohba *et al.*, 1978). In Fig. 3 the interaction of the lone pair of the O1 atom with the positively charged Li atom is also shown. Assuming that the CC associated with the O1-atom lone pair is not easily displaceable, it is interesting to note that the position of the Li atom is such as to maximize the interaction with the six O atoms around it (two are shown in Fig. 3). The very low values of ρ_b and $\nabla^2\rho_b$ for the C—H···O interactions, even if significant from a statistical point of view, are at the limit of experimental accuracy. This fact reflects the qualitative agreement between experimental and theoretical densities in the description of the hydrogen bonds, while it does not invalidate the ability of the topological analysis in also describing the intermolecular interactions. In fact, it is worth noting that almost perfect correspondence of theoretical and experimental results was found in the case of the much stronger N—H···O hydrogen bonds of the L-alanine crystal (Gatti *et al.*, 1992).

Table 5. *Atomic populations (electrons)*

		RHF/3-21G*	
	Multipole	Mulliken	QTAM
C1	6.25 (6)	6.44	
C2	5.92 (11)	6.48	
N1	7.25 (3)	6.50	6.39
N2	7.31 (5)	7.69	
O1	8.12 (3)	8.55	8.73
O2	8.19 (2)	8.55	8.66
Co	24.77 (7)	25.13	25.27
Co *d*-electrons	6.52 (7)	6.52	
Li	2.48 (2)	2.53	2.07
H11	0.93 (3)	0.75	
H12	0.77 (4)	0.73	
H21	0.92 (5)	0.74	

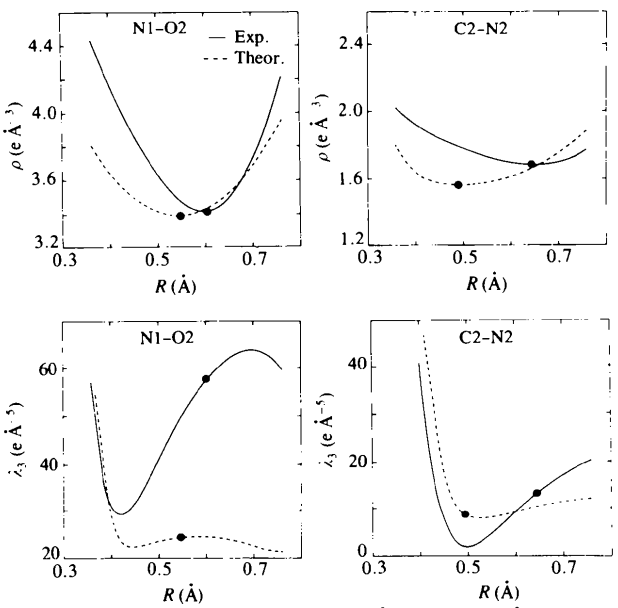

Fig. 5. Experimental and theoretical ρ (e Å^{-3}) and λ_3 (e Å^{-5}) values along the A—B bond path. R (Å) denotes the distance from A, while the dot indicates the BCP position.

3.3. *Electron populations*

The experimental and theoretical atomic electron populations are reported in Table 5. The latter were evaluated with the Mulliken approach and for the Co, Li and NO_2^- subsystems, also according to QTAM. The Co and Li atoms appear generally less charged than anticipated from their formal charges. The QTAM value for the Li atoms is, however, very close (+0.93 e) to that of the ion, in significant agreement with the chemical expectation. The experimental charge on the Co atom is +2.23 (7) e and it is comparable to the RHF/3-21G* Mulliken and QTAM values of +1.87 and 1.73 e, respectively. The charge of the NO_2^- group is −0.56 (5), −0.60 and −0.78 e for experimental, Mulliken and QTAM estimates, respectively. At variance with experiment, QTAM predicts O1 slightly more negatively charged than O2. The greater charge on O1 agrees with the dominance of the resonant structure of the NO_2^- group with N1 and O1 atoms involved in a formal single bond. The net charge of the $[Co(NO_2)_6]$ group is −1.13, −1.73 and −2.95 e for experimental, Mulliken and QTAM estimates,

respectively. The two theoretical results differ by more than one electron, in spite of the fact that they are derived from the same wavefunction. The definition of an atomic population as the expectation value of a quantum observable (Bader & Zou, 1992) gives a result which is in perfect agreement with the formal charge for the ion.

4. Conclusions

The experimental electron distribution shows the same number and type of critical point in the $\rho(\mathbf{r})$ field as found in theory. Thus, the topology of the charge distribution and the *structure* it defines are unaffected by their experimental or theoretical origin; for example, even the weak C—H···O interactions between the tetramethylammonium cations and the nitro group anions are recovered by the two models. This study also shows that there is an agreement between experiment and theory in describing the *nature* of both intra- and intermolecular interactions. However, in some cases the agreement appears to be *qualitative* rather than *quantitative*. In particular, serious differences were found in the case of the Laplacian and of the parallel curvature (λ_3) values for the C—N and N—O interactions. Along the N—O bond path (Fig. 5) the discrepancy between experiment and theory is not essentially due to a different BCP location, but, more importantly, it arises from a much larger experimental λ_3 curvature in a wide interval around BCP's.

The electron density of 3*d*-electrons is aspherical owing to the ligand field; a close parallel between the orbital model description, adopted in previous studies on Co^{III} complexes, and the shape of the Laplacian distribution around the Co atom is outlined. Therefore, the conclusions which were drawn previously from the orbital model and the deformation density are now supported by an analysis directly performed on physical observables.

It is a remarkable result that the net charges of Li^+ and $[Co(NO_2)]^{3-}$ ions derived from QTAM are very close to the formal ones. The theoretical and experimental net charges for these ions, respectively derived from the Mulliken method and monopole populations, are relatively similar to each other, but much smaller than QTAM estimates, and at variance with those expected on the basis of chemical intuition.

One of us (CG) acknowledges the support by the Human Capital and Mobility programme of the European Community under Contract No. CHRX-CT93-0155. The help of Mr M. Bandera in preparing the drawings is gratefully acknowledged.

References

Adovasio, V., Lina, F., Nardelli, M. & Pelizzi, F. (1994). *Acta Cryst.* C**50**, 871-874.

Bader, R. F. W. (1990). *Atom in Molecules: A Quantum Theory*, Vol. 22. Oxford: International Series of Monographs on Chemistry.

Bader, R. F. W. & Essen, H. (1984) *J. Chem. Phys.* **80**, 1943-1959.

Bader, R. F. W. & Zou, P. F. (1992). *Chem. Phys. Lett.* **191**, 54-58.

Bader, R. F. W., Slee, T. S., Cremer, D. & Kraka, E. (1983). *J. Am. Chem. Soc.* **105**, 5061-5068.

Clementi, E. & Roetti, C. (1974). *At. Data Nucl. Data Tables* **14**, 177-478.

Dovesi, R., Saunders, V. R. & Roetti, C. (1992). *CRYSTAL92 User Documentation*. University of Torino.

Gatti, C., Bianchi, R., Destro, R. & Merati, F. (1992). *J. Mol. Struct. (Theochem.)* **255**, 409-433.

Gatti, C., MacDougall, P. J. & Bader, R. F. W. (1988). *J. Chem. Phys.* **88**, 3792-3804.

Gatti, C., Saunders, V. R. & Roetti, C. (1993). *5th International Conference on the Applications of the Density Functional Theory in Chemistry and Physics*, p. 83. Como (Italy), 13-16 September.

Gatti, C., Saunders, V. R. & Roetti, C. (1994). *J. Chem. Phys.* **101**, 10686-10696.

Hehre, W. J., Ditchfield, R., Stewart, R. F. & Pople, J. A. (1970). *J. Chem. Phys.* **51**, 2769-2773.

Hehre, W. J., Radom, L., Schleyer, P. V. R. & Pople, J. A. (1986). *Ab Initio Molecular Orbital Theory*. New York: Wiley.

Howard, S. T., Hursthouse, M. B., Lehmann, C. W. & Poyner, E. A. (1995). *Acta Cryst.* B**51**, 328-337.

Iwata, M. & Saito, Y. (1973). *Acta Cryst.* B**29**, 822-832.

Johnson, C. K. (1976). *ORTEP*II. Report ORNL-5138. Oak Ridge National Laboratory, Tennessee, USA.,

Morooka, M., Ohba, S., Saito, Y. & Miyamae, H. (1991). *Acta Cryst.* B**47**, 910-917.

Ohba, S., Toriumi, K., Sato, S. & Saito, Y. (1978). *Acta Cryst.* B**34**, 3535-3542.

Pisani, C., Dovesi, R. & Roetti, C. (1988). Hartree-Fock *ab initio* treatment of crystalline systems, *Lecture Notes in Chemistry*, Vol. 48. Berlin: Springer.

Ruedenberg, K. & Schwarz, W. H. E. (1990). *J. Chem. Phys.* **92**, 4956-4969.

Saito, Y. (1979). *Inorganic Molecular Dissymmetry*. New York: Springer-Verlag.

Stewart, R. F. (1976). *Acta Cryst.* A**32**, 565-574.

Stewart, R. F. & Spackman, M. A. (1983). *VALRAY User's Manual*. Department of Chemistry, Carnegie-Mellon University, Pittsburgh.

Tsirelson, V. G., Zou, P. F., Tang, T. H. & Bader, R. F. W. (1995). *Acta Cryst.* A**51**, 143-153.